

# Two-dimensional Floquet stability analysis of the flow produced by an oscillating circular cylinder in quiescent fluid

John R. Elston<sup>a</sup>, John Sheridan<sup>a</sup>, H.M. Blackburn<sup>b,\*</sup>

<sup>a</sup> *Department of Mechanical Engineering, Monash University 3800, Australia*

<sup>b</sup> *CSIRO Manufacturing & Infrastructure Technology, PO Box 56, Highett 3190, Australia*

Received 31 March 2003; accepted 29 May 2003

---

## Abstract

We study the two-dimensional symmetry breaking transitions in the time-periodic flow generated in quiescent fluid by a rigid cylinder with simple harmonic rectilinear translation in a direction normal to its axis. The base flow possesses two symmetries: a spatio-temporal symmetry and a spatial reflection symmetry about the axis of oscillation. Two distinct regimes of marginal stability are identified through two-dimensional Floquet analysis. These correspond to (I) a pair of real Floquet multipliers simultaneously crossing the unit circle at  $\mu = +1$  and (II) a pair of complex-conjugate multipliers crossing the unit circle,  $\mu = e^{\pm i\theta}$  (a Neimark–Sacker bifurcation). In both transitions the spatial reflection symmetry of the base flow is broken, but for type I transitions, the spatio-temporal symmetry of the base flow is retained.

© 2003 Elsevier SAS. All rights reserved.

*Keywords:* Oscillating circular cylinder; Symmetry breaking; Floquet analysis; Neimark–Sacker bifurcation

---

## 1. Introduction

The stability of flow generated in quiescent fluid by the rectilinear sinusoidal oscillation of a circular cylinder in a direction normal to its axis has been the subject of both experimental studies [1–4] and also two-dimensional numerical investigations [5]. The flow is of fundamental interest, and results have potential application to the study of loads on structures immersed in waves or other oscillatory flows.

Two dimensionless control parameters determine the state of this flow. These are the Keulegan–Carpenter number,  $KC = 2\pi A/D$ , and the Stokes number,  $\beta = D^2/\nu T$ , where  $A$  is the amplitude of motion,  $D$  is the cylinder diameter,  $T$  is the period of oscillation, and  $\nu$  is the kinematic viscosity of the fluid. At low values of  $KC$  and  $\beta$ , the periodic flow is two-dimensional. The visual observations of Honji [1] and Tatsuno and Bearman [3] demonstrated that the symmetry breaking transitions from the base flow occur through instabilities that have both two-dimensional and three-dimensional aspects. In previous work [6], we have addressed some of the three-dimensional instabilities, using three-dimensional Floquet analysis. That work also helped establish that some of the transitions, noted to be primarily two-dimensional in nature [3], are located quite accurately in  $(KC, \beta)$  control space when simulations are restricted to two space dimensions. While the two-dimensional flows are sometimes first unstable to three-dimensional perturbations, these instabilities do not appear to significantly influence the primarily two-dimensional symmetry-breaking transitions. In the present work, we restrict attention to two-dimensional bifurcations, and employ two-dimensional Floquet analysis.

---

\* Corresponding author.

*E-mail address:* [hugh.blackburn@csiro.au](mailto:hugh.blackburn@csiro.au) (H. Blackburn).

The base flows have two two-dimensional symmetries. If the direction of motion of the cylinder is taken to be parallel to the  $y$  axis, and the flow  $(U, V)$  is generated in the  $(x, y)$  plane, the two symmetries possessed by this base flow are the spatial reflection symmetry (reflection about  $y = 0$ )

$$(U, V)(x, y, t) = (-U, V)(-x, y, t), \quad (1)$$

and the spatio-temporal symmetry

$$(U, V)(x, y, t) = (U, -V)(x, -y, t + T/2). \quad (2)$$

Our computations are all performed using primitive variables (velocity, pressure), but as visualisations will be presented in the form of vorticity contours, note that the corresponding symmetries for the out-of-plane vorticity component  $\Omega$  are

$$\Omega(x, y, t) = -\Omega(-x, y, t), \quad (3)$$

$$\Omega(x, y, t) = -\Omega(x, -y, t + T/2). \quad (4)$$

Fig. 1 shows base flows at two points in  $(KC, \beta)$  control space, and serves to illustrate their reflection symmetry (3).

Three types of flows which break the two-dimensional reflection symmetry (1), (3) have previously been observed both in experiment and in two-dimensional direct numerical simulation (DNS) studies; these are exemplified in Fig. 2, which shows instantaneous vorticity contours from two-dimensional DNS. At comparatively small values of  $\beta$ , the transition with increasing  $KC$  is to a synchronous state (with period close to that of the base flow); this is illustrated in Fig. 2(a) – the transition breaks the reflection symmetry but not the spatio-temporal symmetry. The sign with which the flow breaks symmetry in the  $x$ -direction is arbitrary (but constant with time), depending on initial conditions. At intermediate values of  $\beta$ , the symmetry breaking that occurs with increasing  $KC$  is to a quasi-periodic state, where the flow ‘flaps’ from side to side and sheds discrete vortices at a secondary period  $T_s$ ; this flow is illustrated in Fig. 2(b). The third kind of flow with broken symmetry (Fig. 2(c)), observed at higher values of  $\beta$ , has a chaotic nature, where, as in Fig. 2(b), discrete vortices are shed, and the flow ‘flaps’ from side to side, but at irregular intervals.

The curves of marginal stability for the two-dimensional symmetry breaking transitions in  $(KC, \beta)$  control space have been approximately established by prior experimental [3] and DNS [6] studies. As can be seen in Fig. 3, the experiments and DNS are in close agreement for the location of the transitions. In addition, this figure shows labels indicating the approximate location of some of the regimes defined by Tatsuno and Bearman [3]. Regimes A and B correspond (in the restriction to two-dimensional flows) to the vorticity contours shown in Fig. 1 (a) and (b), respectively, while regimes D, C and E are represented by the vorticity contours of Fig. 2 (a), (b) and (c), respectively.

In the remainder of this work, we investigate two-dimensional bifurcations which break the pair of symmetries exhibited by the base flows via two-dimensional Floquet analysis, and obtain the loci in  $(KC, \beta)$  control space of two kinds of two-dimensional symmetry breaking bifurcations. The maximum Stokes number for the present investigations is  $\beta = 100$ , and the maximum Keulegan–Carpenter number is  $KC = 10$ .

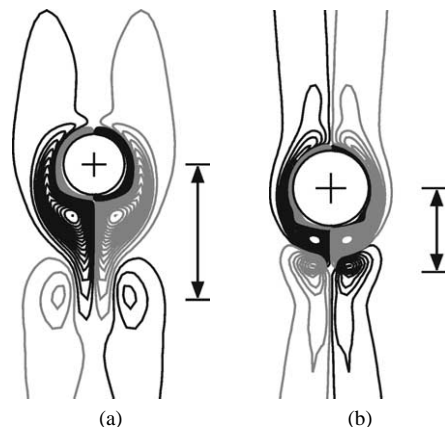


Fig. 1. Illustration of instantaneous vorticity contours for the base flows at (a)  $(KC = 7.0, \beta = 12.5)$ , and (b)  $(KC = 3.5, \beta = 100)$ . The flows are shown at the instant of maximum travel in the vertical ( $y$ ) direction, with the extent of peak-to-peak travel shown. Positive vorticity indicated by black contours, negative by grey.

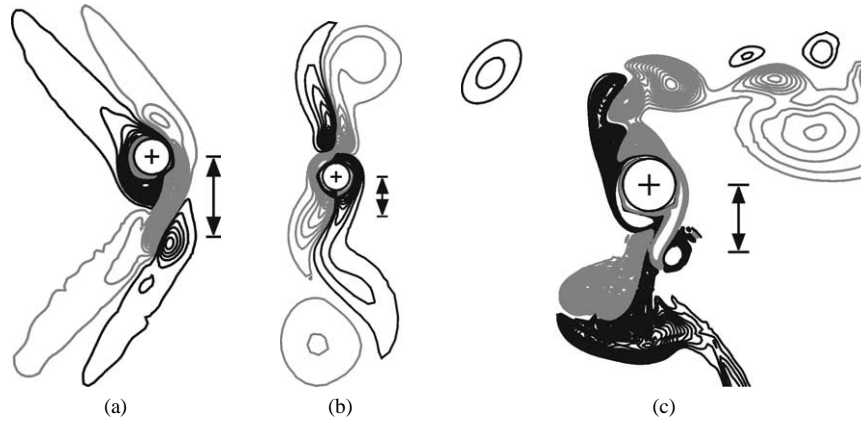


Fig. 2. Instantaneous vorticity contours from two-dimensional DNS, illustrating three variations in transition from the symmetrical base flows: (a) Synchronous ( $T$ -periodic) regime, shown at ( $KC = 7, \beta = 13.5$ ); (b) quasi-periodic regime, shown at ( $KC = 5, \beta = 40$ ); (c) chaotic regime, shown at ( $KC = 4, \beta = 100$ ).

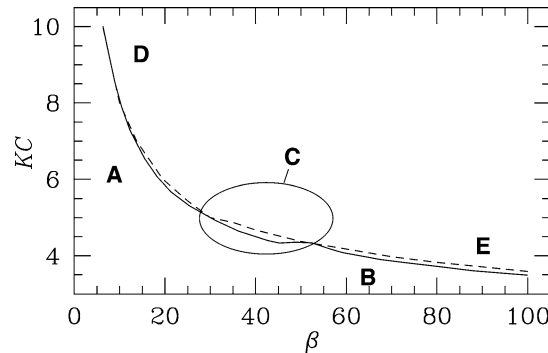


Fig. 3. Boundaries between the two-dimensional symmetrical flows and those with broken symmetry, as established in the experiments of Tatsuno and Bearman [3] (solid line) and two-dimensional DNS [6] (dashed line): above the lines, the flow breaks two-dimensional reflection symmetry (1), (3). Labels A–E indicate approximately the locations of various flow regimes identified in [3].

## 2. Computational methodology

In Floquet stability analysis [7] a  $T$ -periodic base flow,  $\mathbf{U}$ , is examined in conjunction with a perturbation,  $\mathbf{u}'$ , to determine whether the perturbation grows or decays in time. The evolution equations for the perturbation flow are the Navier–Stokes equations linearised about the base flow. Perturbation solutions,  $\mathbf{u}'$ , can be written as a sum of components  $\tilde{\mathbf{u}}(t_0) \exp \sigma(t - t_0)$  where  $\tilde{\mathbf{u}}(t_0)$  is a  $T$ -periodic Floquet eigenfunction, evaluated at arbitrary phase  $t_0$ , and  $\sigma$  is a Floquet exponent. Floquet multipliers  $\mu$  are related to the Floquet exponents  $\sigma$  by  $\mu = \exp \sigma T$ . In general, the exponents  $\sigma$  and the multipliers  $\mu$  can either be real, or occur in complex-conjugate pairs. Instability occurs when a multiplier leaves the unit circle ( $|\mu| \geq 1$ ), or equivalently when the real part of a Floquet exponent becomes positive.

The technique used here for Floquet analysis is a Krylov subspace method that examines the stability of the linearised Poincaré map for the perturbation flow, and is detailed in [8]. Other applications of the numerical method may be found in [9–11]. These previous applications have been to three-dimensional perturbation flows, and where the flow boundaries have either been locations of zero local acceleration of the base flow, or solid walls; a restriction to two spatial dimensions, and application to a domain where the local acceleration of the base flow is non-zero on far-field boundaries, entails some modification and special considerations, outlined below.

The base flow to be tested for stability is obtained by solving the two-dimensional incompressible Navier–Stokes equations in an accelerating reference frame, attached to the cylinder [12,13]. The reflection symmetry (1) of the base flow is enforced by solving in a half domain (see Fig. 4(a)), with symmetry boundary conditions along the  $x = 0$  boundary. The base flow obtained in this way is integrated in time until it reaches a periodic state, after which it is projected (by reflection in the line  $x = 0$ ) onto the full domain mesh Fig. 4(b), and stored for Fourier time interpolation. Typically 64 time slices, equi-spaced in time over the base flow period  $T$ , are used by the Floquet solver for this reconstruction of the base flow.

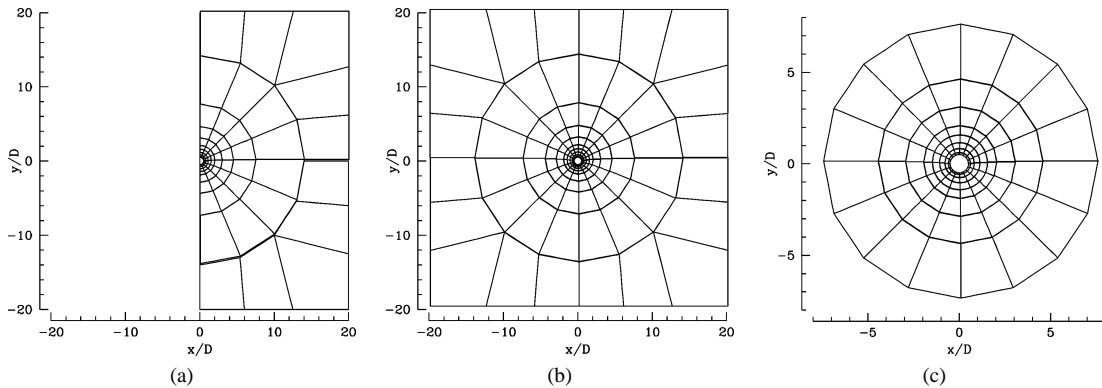


Fig. 4. Domains and spectral element meshes used for computations. The centre panel, (b), shows the 164-element  $40D \times 40D$  domain, used for Floquet stability calculations; panel (a) shows the corresponding half-domain used to produce symmetrical periodic base flow fields, while (c) illustrates a sub-domain used to examine domain size effects on Floquet analysis.

Table 1

Convergence results for Floquet multipliers at (a) different polynomial interpolant orders with a  $40D \times 40D$  domain, where  $p$  is the order of the tensor-product interpolant function employed within each spectral element; (b) different domain sizes at  $p = 8$ . All simulations were conducted at ( $KC = 3.65$ ,  $\beta = 100.0$ )

(a)	$p$	6	8	10	12
	$ \mu $	1.147180	1.147338	1.147052	1.146481
(b)	Domain size	$20D \times 20D$	$40D \times 40D$	$60D \times 60D$	$80D \times 80D$
	$ \mu $	1.110241	1.147338	1.144826	1.142876

The boundary conditions applied to the velocity perturbation are  $u' = 0$  on all domain boundaries. This is a suitable boundary condition for the symmetry breaking Floquet modes, however these boundary conditions are not suitable for resolving the mode of marginal stability ( $\mu = +1$ ) that can exist in a Floquet analysis [7]: in the current problem, this mode represents the local acceleration field ( $\partial_t \mathbf{U}$ ) of the base flow at  $t = t_0$ , which in general is non-zero on the far-field boundary. In practice, this incompatibility means that the method has difficulty resolving modes for which  $|\mu| \leq 1$ , however, it is successfully able to resolve unstable two-dimensional modes, i.e., for  $|\mu| > 1$ .

Spatial discretisation was carried out with spectral elements, with Lagrange interpolant shape functions based on Gauss–Lobatto–Legendre quadrature points. Interpolant order and domain size selections were carried out on the basis of convergence results for Floquet multipliers at ( $KC = 3.65$ ,  $\beta = 100.0$ ) and summarised in Table 1: a polynomial interpolant order  $p = 8$  and a domain size of  $40D \times 40D$  were selected for subsequent work. The domain size corresponds approximately to that used in experiments of Tatsuno and Bearman [3]. As a further check of domain size effects, an analysis was carried out using a much smaller domain (Fig. 4(c)), with the base flow computed on the  $40D \times 40D$  domain and projected onto this smaller domain); the resulting variation in  $|\mu|$  was less than 0.3%, confirming that Floquet mode energy is concentrated near the cylinder.

### 3. Results

Our investigation has determined that there is a single curve of marginal stability for the initial two-dimensional symmetry breaking transitions, but the bifurcations on it fall into two distinct regimes. These two regimes correspond to (I) real Floquet multipliers crossing the unit circle at  $\mu = +1$  (synchronous modes) and (II) complex-conjugate pairs of multipliers crossing the unit circle (quasi-periodic modes). We examine these two types of instability and their relation to the three types of symmetry breaking behaviour found previously (Fig. 2) in the following sections.

#### 3.1. Synchronous modes

The transition to synchronous flows with broken reflection symmetry (1), (3) occurs at comparatively low values of  $\beta$ , and high values of  $KC$ . In Fig. 5(a) we see instantaneous vorticity contours for the base flow at ( $KC = 7.0$ ,  $\beta = 13.5$ ) for the time at which the cylinder is at its maximum displacement in the  $y$  direction. Fig. 5(b) shows the vorticity contours of a critical Floquet eigenfunction at the same phase in the motion cycle. The eigenfunction breaks the reflection symmetry (3), and so does the

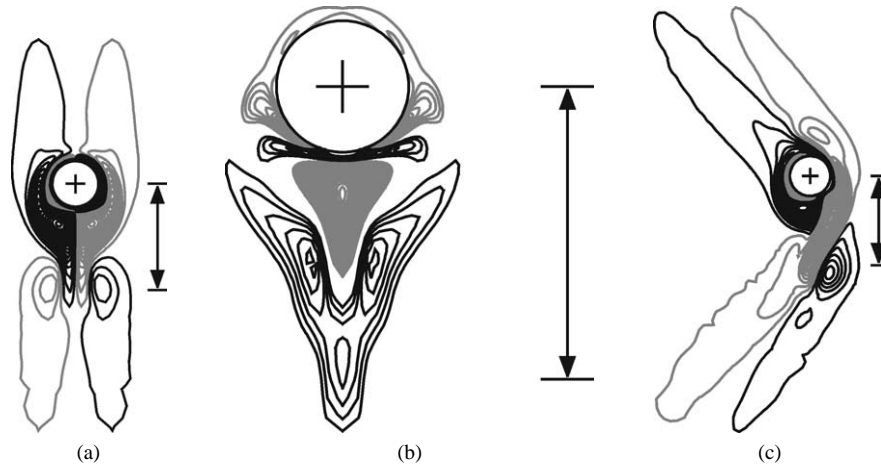


Fig. 5. Vorticity contours illustrating a synchronous symmetry-breaking transition: (a) periodic base flow at ( $KC = 7.0$ ,  $\beta = 13.5$ ); (b) one of the symmetrically related pair of marginally stable Floquet eigenfunction at the same set of control parameters; (c) DNS result at ( $KC = 7.0$ ,  $\beta = 15.0$ ).

resulting flow. In Fig. 5(c) we show vorticity contours for a the saturated flow obtained at a slightly larger value of  $\beta$ , computed using DNS initiated with the base flow perturbed by the leading Floquet eigenfunction.

The eigenfunction varies with phase in the motion cycle, and while it breaks reflection symmetry (3), it retains the spatio-temporal symmetry (4), as does the perturbed flow. As the reflection symmetry can break in two ways, the unstable Floquet modes come in left- and right-handed pairs, and there is correspondingly a pair of Floquet multipliers that cross the unit circle simultaneously at  $\mu = +1$ .

The synchronous symmetry breaking appears to correspond well to the flow visualisation results presented for the transition  $A \rightarrow D$ , as described in [3]. Regime D is also known as the ‘transverse street’ regime [2].

### 3.2. Quasi-periodic modes

At higher values of  $\beta$ , the first Floquet multipliers to cross the unit circle occur in complex-conjugate pairs, i.e.  $\mu = e^{\pm i\theta}$ , so the bifurcation is of Neimark–Sacker type [14]. A secondary period,  $T_S$ , arises, so the resulting flows are – initially at least – quasi-periodic, and evolve on 2-tori. While in general the new period is not necessarily simply related to  $\theta$  (which is not a self-rotation number), in the cases examined here, we find  $T_S = 2\pi T/\theta$ . Both the Floquet multipliers and their eigenfunctions arise in complex-conjugate pairs, but it is sufficient to examine either the real or imaginary parts of the eigenfunctions, as one can be obtained from the other by evolution in time by  $T_S/4$  [11]. Again, the eigenfunctions break the reflection symmetry of the base flow about the oscillation axis, and owing to the quasiperiodic nature of the solutions, the spatio-temporal symmetry is broken as well.

At moderate values of  $\beta$  and  $KC$  (corresponding to the the transition  $A \rightarrow C$  in Fig. 3), the saturated flow at ( $KC$ ,  $\beta$ ) values slightly above critical evolves to a quasi-periodic state, where the secondary period  $T_S$  is linked to a slow flapping  $+x \rightarrow -x$  of the induced flow, and the shedding of discrete vortices. This behaviour is illustrated in Fig. 6, which shows the base flow and (real part) Floquet eigenfunction at ( $KC = 4.60$ ,  $\beta = 40.0$ ), together with a snapshot of the quasi-periodic flow observed at ( $KC = 4.60$ ,  $\beta = 44.2$ ).

In order to establish the linkage between the phase angle  $\theta$  obtained through Floquet analysis and the secondary period  $T_S$ , spectral analysis of quasi-periodic time-series data (force exerted on the cylinder in DNS) was carried out, and  $T_S$  extracted. Fig. 7(a) illustrates the variation of  $|\mu|$  with  $KC$  at  $\beta = 44.2$ : below  $KC_C = 4.515$ , the mode of marginal stability is the leading mode, while for  $KC > KC_C$ ,  $|\mu|$  increases approximately linearly with  $KC$ . At  $KC_C$ , the Floquet multiplier phase angle,  $\theta \simeq 0.5$ , and  $\theta \rightarrow 0$  with increasing  $KC$  (Fig. 7(b)). In Fig. 7(c) the secondary period computed simply from  $T_S = 2\pi T/\theta$  is shown, and compared to the secondary period computed from spectral analysis of the DNS data: it can be seen that at criticality, the two periods match. As  $T_S/T \sim 13$ , the vortex shedding period is clearly much longer than the cylinder oscillation period.

The Stokes number chosen for the above analysis,  $\beta = 44.2$ , corresponds to one of the flow visualisations (Fig. 13) in [3], which clearly exhibits periodic vortex shedding, nominally similar to the flow illustrated in Fig. 6(c). Although the Keulegan–Carpenter numbers differ slightly ( $KC = 4.40$  in [3] compared to  $KC_C = 4.515$  here), and the results in [3] suggest that the flow is subsequently unstable to three-dimensional secondary instabilities, this agreement in two-dimensional flow structure for the transition  $A \rightarrow C$  is significant and reassuring. As was noted in [3], the sense of rotation of the shed vortices is the opposite

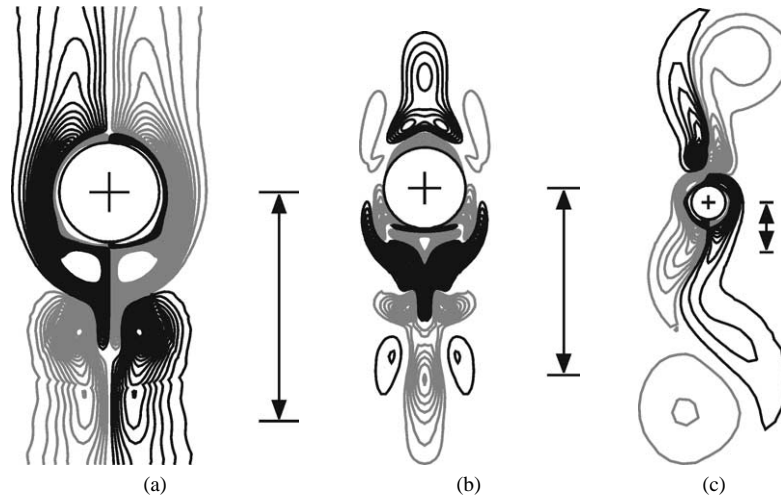


Fig. 6. Vorticity contours for a transition across the critical transition curve from regime A to C. Shown are: (a) periodic base flow at ( $KC = 4.60$ ,  $\beta = 40.0$ ); (b) the real part of one of the complex-conjugate pair of critical Floquet modes at ( $KC = 4.60$ ,  $\beta = 40.0$ ); (c) DNS results at ( $KC = 4.60$ ,  $\beta = 44.2$ ).

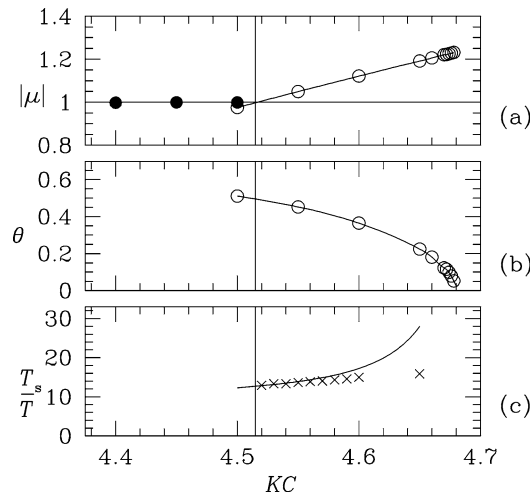


Fig. 7. Illustration of the Neimark–Sacker bifurcation that occurs at  $\beta = 44.2$ . In (a) the variation of  $|\mu|$  with  $KC$  is plotted: solid circles represent multipliers for the mode of marginal stability corresponding to  $\partial_t \mathbf{U}$ , while open circles show magnitudes for a complex-conjugate pair of multipliers that cross the unit circle at  $KC = 4.515$ . In (b) the phase angle for the complex-conjugate pair of multipliers is plotted, while in (c) the secondary periods computed from  $T_s = 2\pi T/\theta$  (solid line) are compared to those obtained from spectral analysis of DNS time-series data ( $\times$ ).

that which would be expected for a wake flow; instead, this is the instability of the jet-like streaming flow, outwards along the oscillation axis.

At higher Stokes numbers (up to  $\beta = 100$ , the limit of our work), the stability analysis again shows that the initial bifurcation from the symmetric base flows occurs through a Neimark–Sacker bifurcation. To illustrate this point, we show in Fig. 8 the variation in magnitude and phase angle of the complex-conjugate pair Floquet multipliers along a traverse of  $KC$  at  $\beta = 80$ . Marginal stability here occurs at  $KC = 3.815$ , and  $\theta \approx 0.82$  at onset.

At the higher Stokes numbers, the linear analysis suggests that the nonlinearly evolved flow should again be quasi-periodic, and this is the case for  $(KC, \beta)$  pairs that lie very close to the linear bifurcation boundary. However, as the control parameters move further from the bifurcation point, the two-dimensional flows become chaotic, as noted in Section 1, and shown in Fig. 2(c). This behaviour may be associated with further instabilities either of the two-dimensional base states, or of the quasi-periodic flows that arise through the Neimark–Sacker bifurcation, or it may be associated with interaction of the shed vortices with the far-field boundaries. We note that the behaviour is similar to that observed for regime E in the experiments of [3].

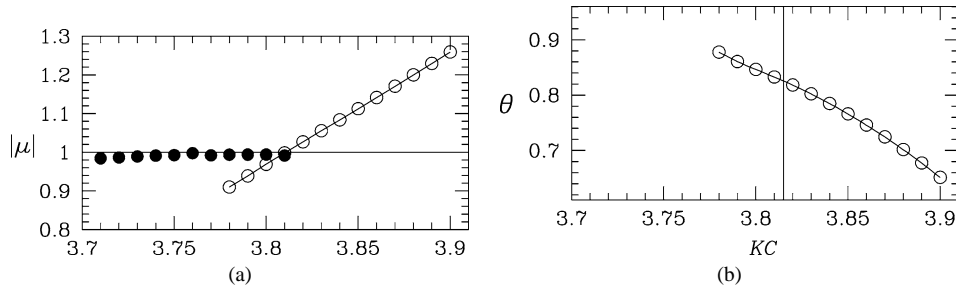


Fig. 8. The Neimark–Sacker bifurcation at  $\beta = 80$ , showing variation of (a)  $|\mu|$  and (b)  $\theta$  with  $KC$ . In (a), filled circles indicate modes with real Floquet multipliers, while open circles indicate modes with complex-conjugate pair multipliers.

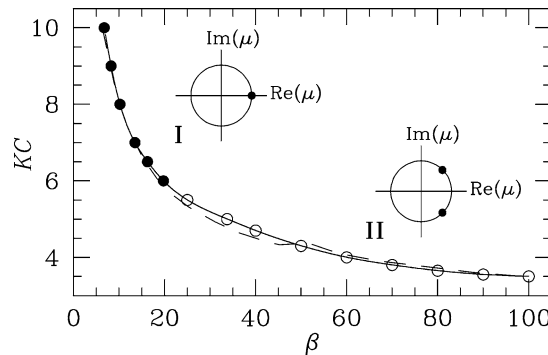


Fig. 9. Diagram illustrating the curve of marginal stability for the two modes of two-dimensional symmetry breaking. The synchronous mode, regime I, which has a pair of real multipliers crossing the unit circle at  $\mu = +1$ , is indicated by  $\bullet$ , the quasi-periodic mode, regime II, with  $\mu = e^{\pm i\theta}$ , by  $\circ$ , while the boundary for the transitions  $A \rightarrow D$ ,  $A \rightarrow C$  and  $B \rightarrow E$  observed in experiments, [3], is indicated by the dashed line.

It should be observed that for the higher Stokes numbers ( $\beta \gtrsim 50$ ), the two-dimensional base flows are first unstable to three-dimensional, rather than two-dimensional, perturbations [3,6] – in reality, regime B has three-dimensional flows – so these two-dimensional instabilities would in fact be secondary ones at high Stokes numbers. Nevertheless, two-dimensional analysis appears to be sufficient to represent the underlying nature of the transition  $B \rightarrow E$ , as well as  $A \rightarrow C$  and  $A \rightarrow D$ .

### 3.3. Control-space locus

The results of our two-dimensional Floquet analyses for this problem are summarized in Fig. 9, which shows the curve of marginal stability for the synchronous and quasi-periodic modes in  $(KC, \beta)$  control space. The location of this curve agrees closely with previous experimental results [3] for the fundamentally two-dimensional transitions. The two regimes shown correspond to the types of bifurcations mentioned previously: (I) a pair of real Floquet multipliers crossing the unit circle at  $\mu = +1$  and (II) a pair of complex-conjugate multipliers crossing the unit circle (a Neimark–Sacker bifurcation). The transition from regime I to II occurs at  $\beta \approx 18$ .

## 4. Conclusions

Two-dimensional Floquet stability analysis of symmetric periodic flows produced by an oscillating circular cylinder accurately predicts the locations in  $(KC, \beta)$  space where two-dimensional symmetry is broken. There is a single curve of marginal stability, but two distinct regimes, which correspond to (I) pairs of real Floquet multipliers crossing the unit circle at  $\mu = +1$ , giving rise to left- and right-handed pairs of synchronous two-dimensional instability modes, and (II) complex-conjugate pairs of multipliers crossing the unit circle, giving rise to quasi-periodic instability modes. Both instabilities break the reflection symmetry of the base flows, while (I) retains their spatio-temporal symmetry. The quasi-periodic modes produce shedding of discrete vortices into the flow – as noted previously [3], these correspond to jet-like, as opposed to wake-like, instability of the streaming flow along the oscillation axis.

We have examined only the initial two-dimensional symmetry-breaking instabilities of these flows (i.e., those which first break symmetry as  $KC$  or  $\beta$  are increased from low values), so there are possibly other modes to which the two-dimensional

symmetrical flows are unstable as  $KC$  or  $\beta$  are further increased. Finally, we note that outside the range of control parameters considered here (particularly at larger  $KC$ ), a number of other primarily two-dimensional instabilities have been reported [2]; these remain to be approached through Floquet analysis.

### Acknowledgements

We thank both the Victorian and Australian Partnerships for Advanced Computing for their support in providing computational resources for this study.

### References

- [1] H. Honji, Streaked flow around an oscillating cylinder, *J. Fluid Mech.* 107 (1981) 509–520.
- [2] C.H.K. Williamson, Sinusoidal flow relative to circular cylinders, *J. Fluid Mech.* 155 (1985) 141–174.
- [3] M. Tatsuno, P.W. Bearman, A visual study of the flow around an oscillating circular cylinder at low Keulegan–Carpenter numbers and low Stokes numbers, *J. Fluid Mech.* 211 (1990) 157–182.
- [4] T. Sarpkaya, Experiments on the stability of sinusoidal flow over a circular cylinder, *J. Fluid Mech.* 457 (2002) 157–180.
- [5] G. Iliadis, P. Anagnostopoulos, Viscous oscillatory flow around a circular cylinder at low Keulegan–Carpenter numbers and frequency parameters, *Int. J. Numer. Methods Fluids* 26 (1998) 403–442.
- [6] J.R. Elston, J. Sheridan, H.M. Blackburn, The transition to three-dimensionality in the flow produced by an oscillating circular cylinder, in: 14th A/Asian Fluid Mech. Conf. Adelaide, Australia, 2001, pp. 319–322.
- [7] G. Iooss, D.D. Joseph, *Elementary Stability and Bifurcation Theory*, 2nd edition, Springer, Berlin, 1990.
- [8] L.S. Tuckerman, D. Barkley, Bifurcation analysis for timesteppers, in: E. Doedel, L.S. Tuckerman (Eds.), *Numerical Methods for Bifurcation Problems and Large-Scale Dynamical Systems*, Springer, 2000, pp. 453–566.
- [9] D. Barkley, R.D. Henderson, Three-dimensional Floquet stability analysis of the wake of a circular cylinder, *J. Fluid Mech.* 322 (1996) 215–241.
- [10] H.M. Blackburn, Three-dimensional instability and state selection in an oscillatory axisymmetric swirling flow, *Phys. Fluids* 14 (11) (2002) 3983–3996.
- [11] H.M. Blackburn, J.M. Lopez, The onset of three-dimensional standing and modulated travelling waves in a periodically driven cavity flow, *J. Fluid Mech.*, in press.
- [12] H.M. Blackburn, R.D. Henderson, A study of two-dimensional flow past an oscillating cylinder, *J. Fluid Mech.* 385 (1999) 255–286.
- [13] H.M. Blackburn, Computational bluff body fluid dynamics and aeroelasticity, in: N.G. Barton, J. Periaux (Eds.), *Coupling of Fluids, Structures and Waves Problems in Aeronautics*, in: *Notes Numer. Fluid Mech.*, Springer, 2003, pp. 10–23.
- [14] Y.A. Kuznetsov, *Elements of Applied Bifurcation Theory*, 2nd edition, Springer, 1998.